Impacts of large-scale atmospheric circulation changes due to winter sea-ice retreat on Black Carbon transport and deposition to the Arctic

Luca Pozzoli[1], Srdan Dobricic[1], Simone Russo[2], and Elisabetta Vignati[1]

[1]European Commission, Joint Research Centre (JRC), Directorate for Energy, Transport and Climate, Air and Climate Unit, Ispra (VA), 21027, Italy

[2]European Commission, Joint Research Centre (JRC), Directorate for Competences, Modelling, Indicators and Impact Evaluation Unit, Ispra (VA), 21027, Italy

Correspondence to: Luca Pozzoli (luca.pozzoli@jrc.ec.europa.eu)

Abstract. Winter warming and sea ice retreat observed in the Arctic in the last decades determine changes of large scale atmospheric circulation pattern that may impact as well the transport of black carbon (BC) to the Arctic and its deposition on the sea ice, with possible feedbacks on the regional and global climate forcing. In this study we developed and applied a new statistical algorithm, based on the Maximum Likelihood Estimate approach, to determine how the changes of three large scale weather patterns (the North Atlantic Oscillation, the Scandinavian Blocking, and the El Nino-Southern Oscillation), associated with winter increasing temperatures and sea ice retreat in the Arctic, impact the transport of BC to the Arctic and its deposition. We found that the three atmospheric patterns together determine a decreasing winter deposition trend of BC between 1980 and 2015 in the Eastern Arctic while they increase BC deposition in the Western Arctic. The increasing trend is mainly due to the more frequent occurrences of stable high pressure systems (atmospheric blocking) near Scandinavia favouring the transport in the lower troposphere of BC from Europe and North Atlantic directly into to the Arctic. The North Atlantic Oscillation has a smaller impact on BC deposition in the Arctic, but determines an increasing BC atmospheric load over the entire Arctic Ocean with increasing BC concentrations in the upper troposphere. The El Nino-Southern Oscillation does not influence significantly the transport and deposition of BC to the Arctic. The results show that changes in atmospheric circulation due to polar atmospheric warming and reduced winter sea ice significantly impacted BC transport and deposition. The anthropogenic emission reductions applied in the last decades were, therefore, crucial to counterbalance the most likely trend of increasing BC pollution in the Arctic.

1 Introduction

The Arctic has warmed during the recent decades more strongly than other regions due to the polar amplification of the global warming signal (Serreze and Barry, 2011). Satellite observations show a decline in summer sea ice extent since the late 1970s with a dramatic acceleration in the last decade. The sea ice is also characterized by increased fraction of thinner and younger sea ice, which is melting during the polar summer (Comiso, 2012; Kwok and Rothrock, 2009; Kwok, 2009;

Maslanik et al., 2011; Rothrock et al., 2008). The rate of change of the Arctic sea ice has been so fast in the last decades, that the expressions "new Arctic" recently started to be used (e.g. Doscher et al., 2014). Also during winter the sea ice cover and concentration changed significantly: a decreasing trend of sea ice concentration in winter months, December-January-February (DJF), for the period 1979-2014, was observed by satellites over the Barents Sea up to a rate of 20% for decade.

5 Several studies investigated how the varying winter sea ice cover over the Barents Sea may further produce hemispheric scale impacts in the atmosphere with changes in the large scale atmospheric circulation (Cohen et al., 2014; Deser et al., 2007; Mori et al., 2014; Overland and Wang, 2010; Petoukhov and Semenov, 2010; Screen et al., 2013; Semenov and Latif, 2015). Dobricic et al. (2016) found that three independent atmospheric patterns, connected to the North Atlantic Oscillation (NAO), the Scandinavian Blocking (SB), and the El Nino Southern Oscillation (ENSO), are directly related to the ongoing

10 sea ice cover shrinkage in the Barents Sea and the hemispheric increase of near-surface temperature. These changes in the ocean-sea ice-atmosphere energy fluxes also impact the large scale atmospheric circulation in the North Hemisphere, as well as the transport of atmospheric pollutants with possible feedbacks on the regional and global climate.

The aim of this study is to estimate how these changes in the large scale circulation patterns of the North Hemisphere in winter could affect the transport of pollutants to the Arctic, and in particular black carbon (BC). BC is a short lived climate

15 pollutant (SLCP) and thus one of the key targets for emission reduction strategies to mitigate the effects of climate change (Shindell et al., 2012). BC plays a key role in the Arctic climate system as it affects the Earth radiative balance through different mechanisms. BC particles directly absorb solar radiation, and above a surface with high albedo, such as snow and sea ice, they warm the atmosphere inside the haze layer and at higher altitudes (Shaw and Stamnes, 1980). On the other hand, the BC may also cool the Arctic climate due to surface dimming and decreased poleward heat flux caused by

20 weakened latitudinal temperature gradient from BC heating of the upper troposphere (Flanner, 2013; Sand et al., 2013a, 2013b; Shindell and Faluvegi, 2009). An indirect BC radiative forcing process is determined by its deposition on snow and ice, which can accelerate their melting. Hadley and Kirchstetter (2012) measured in laboratory how BC snow contamination can reduce snow albedo, with amplified BC radiative perturbation in larger snow grains size, which is also consistent with the parameterizations of BC and soot concentrations in snow included in climate models (Aoki et al., 2000; Flanner and

25 Zender, 2006; Yasunari et al., 2011). Due to lower insolation in the Arctic during winter and early spring, BC exerts a negligible radiative forcing, but particles that deposit to snow and ice surfaces can re-emerge at the surface when melt commences in the summer (Conway et al., 1996), meaning that winter transport and deposition of BC is also affecting the Arctic climate.

Measurements showed that the BC surface concentrations in the Arctic, as well as those of other atmospheric pollutants, are

30 largest in winter, when the transport of pollutants from lower latitudes is more efficient and the removal processes slower. The extreme cold surface temperatures in the Arctic determine strong inversions building the so-called polar dome (Klonecki, 2003; Stohl, 2006), characterized by stable air masses inside the dome and limited exchange between the boundary layer and the free troposphere, meaning that in the Arctic local sources of pollution are transported more efficiently. On the other hand the long range transport of BC from lower latitudes may contribute more to the Arctic Haze

due to the significantly larger mid-latitudes emission levels compared to those in the Arctic region (Sand et al., 2015). Another barrier which isolate the Arctic from the lower latitudes is the Arctic front (Barrie, 1986). Polluted air masses can reach the Arctic lower troposphere only if they are emitted in a sufficiently cold region located north of Arctic front, situation which mainly occurs during winter in north Eurasia. Pollution emitted south of the Arctic front is lifted above it,

5   with cloud formation and precipitation with deposition to the surface. Pollutants emitted in North America and East Asia can reach the Arctic mainly through this pathway (Stohl, 2006). As a result the main contribution to winter BC concentrations and deposition in the Arctic are originated from northern Eurasia (Hirdman et al., 2010). The BC concentration and deposition vary considerably also on inter-annual time scale, and large scale atmospheric circulation processes can favour or reduce the transport of pollutants from the main source regions (North America and Eurasia) toward the Arctic. Hirdman et

10   al. (2010) analysed the long-term trends of BC and sulphate measured at three stations in the Arctic. They found that BC surface concentrations decreased at two Arctic stations, Alert (Canada) and Zeppelin (Svalbard islands, Norway), while there is no trend detectable at Barrow (Alaska). Analysing the atmospheric back trajectories at the three stations, they concluded that the observed decreasing trends are mainly driven by changes in the emissions, while the impact of atmospheric circulation can only explain a minor fraction of the downward trend. They found significant correlations

15   between the north Atlantic Oscillation Index (NAOI) and air masses from North America and North Eurasia at both Alert and Barrow, but not for the station at Zeppelin. However, the full understanding of how the transport changes related to large scale circulation patterns, such as the NAO, impact the BC concentrations and deposition to the Arctic has not yet been established.

In this study we apply a novel statistical methodology, based on a Bayesian approach, to investigate the relationships

20   between large scale atmospheric circulation patterns and the long range atmospheric transport of air pollutants to the Arctic in recent decades. We estimate the most likelihood BC distribution associated to three large scale atmospheric patterns which mainly contribute the winter near surface warming and sea ice retreat in the Arctic (Dobricic et al., 2016). The distributions of BC surface concentration, total column and deposition fluxes were taken from a hindcast simulation of tropospheric chemistry composition for the period 1980-2005. Three different BC simulations are analysed, one with changing

25   anthropogenic emissions for the entire period, and two with fixed anthropogenic emissions of the year 1980 and 2000, respectively. With this methodology we aim to quantify the trends and inter-annual variability of BC surface concentrations, load and deposition in the Arctic associated with winter large scale atmospheric circulation changes occurred in the last decades.

2 Methods and data

30   In the following sections we will first describe the statistical method (Section 2.1) and the data used for the analysis. Section 2.2 provides a short introduction of the large scale atmospheric patterns identified by (Dobricic et al., 2016), which are

mainly contributed to the winter polar warming of the last decades. Section 2.3 describes the data used to estimate the maximum likelihood distribution of BC concentration and deposition associated to the specific atmospheric patterns.

2.1 Maximum Likelihood Estimate of atmospheric pollutants

The Maximum Likelihood Estimate (MLE) of the distribution of a pollutant in the atmosphere associated to a specific
5 atmospheric pattern may be derived starting from the Bayes theorem. The probability, *p(c/a)*, of an unknown joint distribution of an atmospheric pollutant and corresponding atmospheric state, **c**, given a specific atmospheric pattern, **a** , may be expressed as:

$$p(\mathbf{c} \,|\, \mathbf{a}) \sqcup p(\mathbf{a} \,|\, \mathbf{c})\, p(\mathbf{c}). \tag{1}$$

where *p(c)* is the priori probability of coupled pollutant distribution (e.g. of atmospheric concentrations, surface deposition
10 or atmospheric burden) coupled with corresponding atmospheric conditions, and *p(a/c)* is the probability that a certain atmospheric pattern (e.g. of surface pressure, geopotential height, wind speed) is associated to the atmospheric state coupled with pollutant distributions. The prior probability, *p(c),* can be estimated for example by using chemistry-climate model simulations of the past or future atmospheric physical parameters and the corresponding coupled chemical composition**s**. In order to simplify the mathematical solution of the problem we assume that the two distributions, *p(a/c)* and *p(c),* are
15 approximately Gaussian, meaning that also their product, *p(c/a)*, will be Gaussian. The assumption can be used to estimate the probability of a pollutant distribution for any atmospheric pattern **a$_k$**, which can be taken for example from an independent atmospheric model simulation, or a specific large scale atmospheric pattern, like the ENSO or the NAO. Equation (1) becomes:

$$p(\mathbf{c} \,|\, \mathbf{a}_k) = const \times \exp\left\{ -\frac{1}{2}[\mathbf{a}_k - H(\mathbf{c})]^T \mathbf{D}^{-1}[\mathbf{a}_k - H(\mathbf{c})] - \frac{1}{2}\mathbf{c}^T \mathbf{C}^{-1}\mathbf{c} \right\}, \tag{2}$$

20 where, **H(c)** is a mapping function between coupled atmospheric states being a part of **c** and the specific atmospheric pattern **a**$_k$ that may be defined over different model grids, **D** is the covariance matrix of the differences between atmospheric anomalies, while **C** is the covariance matrix of the coupled atmosphere and pollutant anomalies.

The Maximum Likelihood Estimate (MLE) of $p(\mathbf{c} \,|\, \mathbf{a}_k)$ is the one with the minimum absolute value of the argument of the exponential function in Equation (2) that is the minimum of the cost function *J*:

$$J = \frac{1}{2}[\mathbf{a}_k - H(\mathbf{c})]^T \mathbf{D}^{-1}[\mathbf{a}_k - H(\mathbf{c})] - \frac{1}{2}\mathbf{c}^T \mathbf{C}^{-1}\mathbf{c}. \tag{3}$$

Assuming that the mapping *H* is linear (e.g. a bilinear interpolation, **H(c) = Hc**), *J* becomes a quadratic function with a single minimum which may be estimated by a linear minimizer. The numerical stability may be further increased by defining a

control subspace $\mathbf{z} = \mathbf{Z}^{+}\mathbf{c}$, where $\mathbf{Z}$ is a square root of $\mathbf{C}$ and the superscript + indicates the generalized inverse. The cost function becomes:

$$J = \frac{1}{2}\left[\mathbf{HZz} - \mathbf{a}_k\right]^T \mathbf{D}^{-1}\left[\mathbf{HZz} - \mathbf{a}_k\right] + \frac{1}{2}\mathbf{z}^T\mathbf{z}$$

(4)

After finding $\mathbf{z}$, the most likelihood coupled anomaly is obtained from:

5   $\mathbf{c} = \mathbf{Zz}$.

(5)

The cost function J is minimized using the quasi-Newton Limited memory Broyden–Fletcher–Goldfarb–Shanno (L-BFGS) minimizer (Byrd et al., 1995). It is assumed that $\mathbf{D}$ is a diagonal matrix and elements along the diagonal have equal variance divided by the area of each grid point. The atmospheric patterns $\mathbf{a}_k$, for which we estimate the maximum likelihood distribution of atmospheric pollutants, are those previously described by Dobricic et al. (2016) and briefly described in

10   Section 2.2. Matrix $\mathbf{C}$ is estimated from coupled anomalies of a multi-year simulation with a coupled atmosphere-chemistry model, described in more details in Section 2.3. Coupled anomalies contain both the atmospheric physical parameters and pollution concentrations. In order to filter out statistically insignificant relationships, the covariance matrix of anomalies is approximated by forming the Empirical Orthogonal Function (EOF) decomposition and by maintaining only EOFs with major eigenvalues. The minimum of the cost function J is found for each winter month (from December to February, DJF)

15   and for each atmospheric pattern $\mathbf{a}_k$, separately.

2.2 Atmospheric patterns

Dobricic et al. (2016) performed an Independent Component Analysis (ICA) of atmospheric reanalysis data finding a link between the observed near surface temperature increase and sea ice retreat in the Arctic during winter and three well-known atmospheric oscillation patterns. Hannachi et al. (2009) proposed to apply the ICA instead of the commonly used EOF in

20   climate studies. The major difference between the two estimates is that ICA does not assume the Gaussian distributions of event probabilities. This property ensures that components are truly independent and not just uncorrelated. In Dobricic et al. (2016) the Fastica algorithm by Hyvärinen and Oja (2000) was applied to extract independent atmospheric components in winter during the period 1980-2015. Details on implementing ICA for large-scale atmospheric processes may be found in Dobricic et al. (2016), here we introduce the main results of their study, which are used as an input for our analysis. Three

25   independent atmospheric patterns were found, and they were named by visually recognizing their similarity to well-known large-scale weather patterns, the North Atlantic Oscillation (NAO), Scandinavian Blocking (SB), and the El Nino-Southern Oscillation (ENSO). The relationship between NAO and SB and the sea ice melting over the Arctic is visible in near-surface temperature trends, the associated warming over the Arctic is the largest over the Barents Sea and west of Greenland. NAO and SB are also characterized by the change in the three dimensional structure of winds, impacting the long range transport

30   of pollutants from emission sources in the middle latitudes to the Arctic. They also impact changes in the vertical stability over the Arctic influencing the deposition of pollutants. Dobricic et al. (2016) obtained consistent results using two different

atmospheric reanalysis, the National Center for Environmental Prediction (NCEP, Kalnay et al., 1996), and ERA-Interim (Dee et al., 2011) from the European Centre for Medium-Range Weather Forecasts (ECMWF). In our study we will estimate the maximum likelihood distribution of BC atmospheric concentration, load and deposition associated to the NAO and SB atmospheric patterns found in Dobricic et al. (2016). The third atmospheric pattern, associated to ENSO, showed weaker

5   connection to the changes seen in near-surface temperature and geopotential height in the Arctic region.

2.3 Atmospheric chemical composition

Concentrations and deposition fluxes of atmospheric pollutants were obtained from simulations of the fully coupled aerosol-chemistry-climate model, ECHAM5-HAMMOZ (Pozzoli et al., 2011), which is composed of the general circulation model ECHAM5, the tropospheric chemistry and aerosol module HAMMOZ (Pozzoli et al., 2008a). The model has been

10   extensively evaluated in previous studies by comparing simulated chemical concentrations and physical parameters to observations (Auvray et al., 2007; Pausata et al., 2012, 2013; Pozzoli et al., 2008a, 2008b; Rast et al., 2014; Stier et al., 2004) and within model inter-comparison studies(Kim et al., 2014; Pan et al., 2015; Tsigaridis et al., 2014). The horizontal resolution of the simulations is about $2.8° \times 2.8°$, with 31 vertical levels from the surface up to 10 hPa. The simulation was forced for the entire period by nudging the reanalysis meteorological fields from the ECMWF ERA-40 re-analysis (Uppala

15   et al., 2005) until 2000 and the operational analyses (IFS cycle-32r2) for the remaining period (2001–2005). The anthropogenic emissions of CO, NOx, and VOCs for the period 1980–2000 are taken from the RETRO inventory (Endresen et al., 2003; Schultz et al., 2007, 2008). The AeroCom hindcast aerosol emission inventory (Diehl et al., 2012) was used for the annual total anthropogenic emissions of primary black carbon (BC), organic carbon (OC) aerosols and sulfur dioxide (SO2). The simulation includes also inter-annual varying biomass burning emissions, from tropical savannah burning,

20   deforestation fires, and mid-and high latitude forest fires published by Schultz et al. (2008). Three different simulations are available for our analysis, a reference simulation with annually varying anthropogenic emissions for the entire simulated period (thereinafter named REF), and two additional simulations with anthropogenic emissions kept constant for the entire period at the levels of the years 1980 and 2000 (thereinafter named FIX1980 and FIX2000). These three simulations will provide the opportunity to have a preliminary estimate of the uncertainty of our findings due to the different emission levels

25   and their geographical distribution used in the different simulations. Other model simulations may be analysed in the future to quantify the uncertainty associated to different chemical mechanisms and physical parameterizations.

3 Results

In this study we will focus on the trends of black carbon transport patterns from North Hemisphere mid-latitudes towards the Arctic during winter months. Trends are calculated by the Sen-Kendall method (Sen, 1968). The statistical significance for

30   all trends is set to the 0.05 level and is estimated by the Mann-Kendall test (Mann, 1945). Areas with significant trends are marked with small grey dots in the figures, except for the trends of atmospheric patterns and maximum likelihood estimates

of BC that have spatially uniform slopes. We first analyse the trends as simulated by a coupled chemistry-climate model under three different anthropogenic emission scenarios (Section 3.1). This first analysis will provide an estimate of the relative contribution of anthropogenic emissions and natural variability to the transport of BC toward the Arctic. In the second part, through the statistical method described in Section 2, the trend associated to the natural variability are further

5   decoupled into the contributions from the North Hemispheric large-scale atmospheric weather patterns (Section 3.2), which were found to be associated to the observed near surface Arctic warming and sea-ice retreat (Dobricic et al., 2016). In Section 3.3 we will illustrate the total trends due to the three independent atmospheric components and their impact on the inter-annual variability of BC wet deposition and load over the Arctic. The statistical method was applied to a combination of different datasets in order to analyse the spread of different solutions obtained using two different atmospheric reanalysis,

10   three different chemistry-climate model simulations, and for different time periods (Section 3.4).

3.1 Total trends of BC simulated by ECHAM5-HAMMOZ

The effects of varying anthropogenic emissions together with natural variability (REF) on BC transport in the Arctic are shown in Figure 1. Decreasing and statistically significant trends are simulated over almost the entire Arctic for dry and wet deposition, as well as surface concentrations. The main reductions occurred in the Eastern part of the Arctic, from the

15   Scandinavian Peninsula along almost all the Russian northern coastline, indicating the important role of the emission reductions occurred in the last decades in Europe and Russia. Annually varying anthropogenic emissions are used for the REF simulation, and the BC anthropogenic emissions remained almost constant globally during the simulated period (1980-2005), 4.9 Tg/year, however large changes occurred in those source regions which are also mainly contributing to the transport of BC to the Arctic (Figure S1). Most of the anthropogenic BC is emitted between 30°N and 60°N, and decreased

20   after the 1990s from about 3 Tg/year to about 2.6 Tg/year after 2000. Above 60°N BC anthropogenic emissions are a small fraction of the total and decreased from 100 to 30 Gg/year. Biomass burning emissions at high latitudes, such as boreal forest fires in Siberia, are comparable to anthropogenic emissions and they slightly increased both at mid-latitudes and above 60°N, with peak years connected to specific meteorological conditions, such as strong ENSO anomalies in 2003 and 1998. Previous studies also showed that the main transport pathway of air pollution to the Arctic in winter is originating from the

25   Eurasian continent (Sharma et al., 2013; Stohl, 2006). Nevertheless, it is interesting to note that an increasing trend of BC burden is simulated over all Western Arctic and also part of Eastern Siberia. A possible explanation for this result can be found in the increasing anthropogenic emissions in East Asia (Figure S1), which is also in agreement with previous findings (Sharma et al., 2013). The REF, FIX2000 and FIX1980 simulations are driven by the same atmospheric reanalysis and annually varying biomass burning emissions. The natural variability, or the changes in large scale circulation patterns which

30   occurred in the last decades, determined a significant increasing trend of BC dry deposition and surface concentrations over the Arctic, BC wet deposition increased over the Canadian Archipelago and Greenland. Both FIX2000 and FIX1980 simulations show similar patterns (Figures 2 and S2), with differences due to the changing geographical distribution of anthropogenic emissions, larger in Europe and North America in 1980, predominant in East Asia in 2000. Both FIX2000 and

FIX1980 simulations do not show a significant trend in BC burden over the Arctic (Figures 2d and S2d), which further confirms the role of anthropogenic emissions in East Asia affecting the transport of air pollution at higher altitudes to the Arctic. In some regions, like the Canadian Archipelago and the western Arctic Ocean, the changes in BC trends due to meteorology and natural variability contribute as much as the changes due to anthropogenic emissions. In the next sections we will further decompose the transport pathways of air pollution to the Arctic associated to the main large scale atmospheric circulation patterns, which are the same that are describing the warming amplification in the polar region and which have characterized the changing climate of the Northern Hemisphere of the last decades.

3.2 Trends of BC due to atmospheric circulation changes

Three large scale atmospheric patterns were identified by Dobricic et al. (2016) as the main drivers of the near surface warming in the polar region. Two of them, NAO and SB, showed statistically significant trends of different atmospheric parameters (e.g., surface temperature, pressure, geopotential height, and wind speed) over the Arctic during the last 36 years (1980-2015). A third pattern similar to ENSO showed a small impact in the Arctic (Dobricic et al., 2016), thus we are not showing its contribution to the total trends. In this section we limit our analysis to trends of MLE of BC wet deposition, concentration and load from the FIX2000 simulation and for the longest period available for the construction of coupled anomalies, 26 years (1980-2005). The trends of BC deposition and load are obtained by multiplying the MLE of the BC field by the trend of the associated atmospheric pattern, from the ICA previously performed by Dobricic et al. (2016). We will not discuss the trends of BC dry deposition as in the ECHAM5-HAMMOZ simulations it is only a small fraction of the total trend of BC deposition in the Arctic (Figures 1b, 2b and S2b).

One atmospheric pattern resembled the North Atlantic Oscillation (NAO), which is normally defined as the difference in sea level pressure between the Azores and Iceland. The sea level pressure as well as vertically integrated internal, kinetic and potential energy patterns found through the ICA by Dobricic et al. (2016) show the formation of a negative phase of the NAO already in December which intensify in January and February. The second pattern resemble to the Scandinavian Blocking (SB), which is occurring when a high pressure anomaly develops over Scandinavia and northwest Russia, with corresponding low pressure anomalies in southwest Europe and central Asia. Figure 3 shows the trends of geopotential height at 850 mbar associated to NAO and SB patterns estimated by the ICA of NCEP atmospheric reanalysis data by Dobricic et al. (2016), while the arrows highlight the tendency of the main atmospheric circulation paths. We can expect that due to the different dynamical structures of NAO and SB they will differently impact the transport and deposition of pollutants from emission areas in the middle latitudes and their deposition rate once they reach the Arctic atmosphere.

The negative phase of the NAO (Figure 3a) forms an anticyclonic anomaly over the large part of the Arctic Ocean and a cyclonic anomaly in the Atlantic. The intensity of westerly winds is decreased in the lower troposphere, with lower transport of pollution from North America across the Atlantic Ocean. On the other hand, the NAO slightly increases the transport of pollution from northwest America towards the Arctic Ocean. The dipole of pressure anomalies over the Pacific Ocean is also favouring the export of polluted air masses from East Asia into North America and the Arctic. Consistently with the

circulation pathways described in Figure 3a, the MLEs of BC wet deposition and load trends related to NAO (Figure 4) show a decreasing trend north of the Eurasian coast and an increasing trend north of America and Greenland. The BC load has a positive trend over most of the Arctic Ocean, Greenland and the Canadian Archipelago, and it is related to the presence of the anticyclonic circulation trend over the pole and the cyclonic trend over the North Atlantic extending over Europe. This

5   pattern, as the negative phase of the NAO, is characterized by weaker westerlies, colder and drier conditions in Scandinavia and Russia, warmer temperatures over Greenland and Canadian Archipelago with higher precipitations and BC deposition. Dynamically it also imposes stable conditions in which the pollution may accumulate in the polar dome over the Arctic. The trends of average BC concentrations at different altitudes above 60°N at four different longitudinal portions (quadrants) of the Arctic (0°-90°E; 90°-180°E; 180°W-90°W; 90°W-0°) are shown in Figure 5. In all the four Arctic quadrants an

10   increasing trend of BC concentrations is estimated at an altitude of about 10 km, near the tropopause. Above the tropopause a shift in the vertical profile of BC concentration is observed, with decreasing trend between the tropopause and 15 km, and increasing trend above 15 km and 70°N. As shown in Dobricic et al. (2016), the evolution of the NAO pattern from December to February is indicating a weakening of the stratospheric vortex linking the tropospheric perturbation with the stratosphere, in agreement with findings by Feldstein and Lee (2014). There is an enhanced mixing anomaly between the

15   troposphere and the stratosphere indicated by increased BC concentrations above and decreased below the tropopause. Near the surface the NAO has a small impact on BC concentrations with few differences in the four Arctic quadrants. Only between 0°-90°E there is a small increasing trend above 70°N, while between 90°E-0° the BC concentrations increase only below 70°N.

The Scandinavian blocking pattern SB (Figure 3b) consists of an anticyclonic centre near Scandinavia and weaker centres of

20   opposite sign over South Western Europe and Siberia/Mongolia. In this case advection changes in the lower troposphere indicated by the arrows favour the larger transport of pollutants from Europe directly to the sea ice covered areas of the Arctic Ocean, while due to the southward position of the anticyclonic anomaly the vertical stability over the Arctic is not changed significantly. The large high pressure anomaly over the North Pacific Ocean decreases the Asian influence on the Arctic. In a dynamically consistent way it advects the warm air from the south to the Barents Sea and the cold air from the

25   Arctic into Siberia. Thus, colder surface temperatures over Russia and Europe are associated with the positive phase of the SB pattern and above average precipitations over South Western Europe, due to advection of moist air from the North Atlantic. This circulation pattern results in an increased transport of pollution from Central Europe directly to the Barents Sea and the Arctic, while the transport from Siberia to the Arctic is suppressed. All estimates of the deposition of BC related to SB show a strong positive trend that extends from the Fram Strait, the Barents and Kara Seas to the central part of the

30   Arctic Ocean (Figure 4). The positive trend of the load spreads over the Norwegian Sea and Scandinavia and it indicates the northward advection of the pollution from Europe towards the Arctic Ocean. The relationship between SB deposition and load trends and the trend of the anticyclonic circulation over Scandinavia is especially evident in February (not shown) when the Scandinavian anticyclone trend is the most pronounced (Dobricic et al., 2016). The vertical structure of the estimated BC concentration trend (Figure 6) shows that in this conditions the maximum concentration trend is located in the lower

troposphere below 3 km and mainly in the first quadrant of the Arctic (0°-90°E). A strong increasing trend is extending from mid latitudes up to 90°N near the surface. However a negative trend is observed over the entire Arctic near the tropopause and above. The SB pattern is associated with a negative phase of the ENSO (La Niña), with colder surface temperature in the equatorial Pacific. The opposite signs of perturbations in the equatorial Pacific and in Scandinavia maintain a planetary wave

5   trapped in the troposphere and compared to the NAO pattern a lower transport to the stratosphere (Dobricic et al., 2016).

3.3 Total trends of BC Maximum Likelihood Estimates

Figure 7 shows the reconstructed total trends of BC wet deposition and load, as the sum of the winter seasonal mean of maximum likelihood estimates associated to three independent atmospheric patterns (NAO, SB and ENSO) multiplied by their temporal trends. The BC wet deposition in winter increased in the last decades due to changing atmospheric circulation

10   over a large part of the polar region. The largest increases were estimated over the Barents Sea, the Kara Sea and the Fram strait, south Greenland, Alaska and the Canadian Archipelago, but the increasing deposition trend extends over most of the Arctic Ocean covered by sea-ice in winter (the grey line in Figure 7 represents the limit of sea-ice and snow covered areas averaged since the 1980s). Decreasing BC wet deposition is estimated over most of Siberia and the Laptev Sea and East Siberian Sea. The trend of atmospheric load of BC reconstructed by the three components shows a net increasing trend over

15   the Arctic north of about 75°N and the decreasing trend over the mid latitudes, except over west Russia, the Scandinavian Peninsula and the Norwegian Sea. The trends reconstructed by the MLE analysis are similar to the trends simulated by the FIX2000 chemistry-climate model simulation (Figure 2a and 2d). In particular wet deposition trends are well represented in terms of both magnitude and spatial distribution. The trend of BC load in the FIX2000 simulation is not significant over the polar region, on the other hand part of the noise was removed from the coupled atmospheric-chemistry anomalies by

20   performing and EOF transformation and retaining only the components with largest eigenvalues.

The temporal variability of the BC deposition anomalies in the period 1980-2015 may be estimated for any area and for each pattern. In particular it is interesting to evaluate the combined and individual impacts of NAO, SB and ENSO patterns on the total BC wet deposition and load over the Arctic Ocean, between 80°N-90°N. Figure 8 shows that the NAO pattern produces deposition anomalies with a smaller inter-annual variability than those driven by the SB pattern. The contribution of ENSO

25   to the total deposition is relevant only in the third quadrant of the Arctic (180°W-90°W), north of the Canadian Archipelago. The largest variability is found in the first quadrant, north of Barents and Kara Seas, up to a factor of 10 larger than the other sectors of the Arctic. Deposition anomalies from the NAO pattern are mostly negative till the year 2000, and after become positive. Those from the SB pattern show a strong increase after the year 2000 that dominates the whole trend from 1980 to 2015, which corresponds well to an acceleration in the winter sea ice decrease rate over the Barents Sea, which is often

30   coupled with the formation of the anticyclonic anomaly over Scandinavia (Cohen et al., 2014; Dobricic et al., 2016; Sato et al., 2014; Screen et al., 2013). Figure 9 shows the temporal contribution of NAO, SB and ENSO patterns to the total BC load over the Arctic quadrants. In this case, the NAO pattern drives the inter-annual variability, with negative values until the late 1990s and positive in the last 15 years. The NAO pattern affects BC load over the entire Arctic in a similar way, while the

contribution of the SB pattern has an opposite trend except for the first quadrant, where it is only a small fraction of the total variability. As discussed in the previous section, the SB pattern increase the transport of BC directly from Central Europe to the Barents and Kara Sea, while it decreases the transport from Siberia. The SB pattern has a negative contribution in the last 10 years in the other parts of the Arctic, and in this regions it can be as large as the NAO contribution. In Figures 8 and 9 we can see that also the temporal variability is partially reconstructed by the applied Bayesian statistical approach. The correlation coefficients between the interannual variability reconstructed by the MLE and the FIX2000 model simulation for the common period 1980-2005, range between 0.35 and 0.4 for BC wet deposition and between 0.14 and 0.41 for BC load over the different sectors of the Arctic.

3.4 Uncertainty of the BC Maximum Likelihood Estimates

In order to test the robustness of the statistical method, we have estimated the MLE of pollutant distributions for a set of 8 combinations of coupled atmospheric reanalysis and BC simulations (Table 1). The NAO, SB, and ENSO atmospheric patterns were estimated through ICA by Dobricic et al. (2016) using two different atmospheric reanalysis of the period 1980-2015, NCEP and ERA-INTERIM. A first set of MLEs combined the atmospheric patterns computed from NCEP and ERA-INTERIM with two global chemistry-climate simulations, which used constant anthropogenic emissions (FIX2000, and FIX1980, see Section 2.3). The MLEs were computed using the simulated pollutant fields for the longest period available, 26 years from 1980 to 2005. The results from NCEP-2000-A have been explained in details in the previous sections.

Figure 10 shows the total trends (NAO+SB+ENSO) of BC wet deposition estimated using the FIX2000 and FIX1980 simulations to build the pollutants and atmospheric coupled anomalies. All the 4 estimates are consistent in terms of geographical distribution, magnitude of the estimated trends and their statistical significance. Consistent results are obtained also for the total trends of BC load (Figure S3 in the supplementary material). Only small differences are due to the two atmospheric reanalysis and the two atmospheric composition simulations, which have a different geographical distribution of anthropogenic emissions (Figure S1).

In a second set of MLEs, we used the REF model simulation, which includes annually varying anthropogenic emissions. In this case, the sudden drop of anthropogenic emissions in Eastern Europe and Russia, and increase in East Asia in the early nineties (Figure S1d), introduced a strong discontinuous change in the transport variability that was impossible to resolve by the statistical method. Thus we chose a shorter period to form the simulated chemistry and atmospheric coupled anomalies, 13 years (1993-2005) after the drop of anthropogenic emissions. Figure 11 shows the estimated trends of BC wet deposition (trends of BC load are shown in Figure S4 of the supplementary material) using only 13 years of coupled anomalies, from the REF simulation and also from the FIX2000 simulation for comparison. Also in this case the results shown in Figures 10 and 11 are consistent, using a shorter period to form the simulated coupled anomalies and with both constant and varying anthropogenic emissions (without large emission changes in a short time). In the most remote Arctic region covered by sea-ice, far from the main anthropogenic sources, the entire set of estimated trends of BC transport and deposition are very close

to each other, meaning that the applied methodology can robustly approximate the transport of pollutants to this region and the trends associated to different large scale circulation patterns.

4 Conclusions

Different studies found significant connections between the winter sea ice retreat in the Arctic observed in the last decades and changes in the large scale atmospheric circulation. Dobricic et al. (2016) estimated that the trend of winter near surface warming of the Northern Hemisphere is well approximated by three independent components which are also very similar to well-known atmospheric oscillations, the NAO, SB, and ENSO. We developed a new statistical algorithm to combine the estimates of NAO, SB and ENSO independent components by Dobricic et al. (2016) with chemistry-climate model simulations of transport and deposition of black carbon (BC) over the Arctic. For a given independent component of the atmospheric variability our algorithm estimates the most likelihood deposition and load of BC consistent with the variability of the atmosphere-chemistry coupled anomalies. To test the robustness of the method and the spread of the possible solutions, the method is applied with two atmospheric reanalysis, NCEP and ERA-INTERIM, and three realizations of coupled anomalies from ECHAM5-HAMMOZ global model simulations, with constant and annually varying anthropogenic emissions.

The main results are summarized in the following points:

- The trends of BC concentrations and deposition fluxes simulated by a global chemistry-climate model (ECHAM5-HAMMOZ) indicated a strong reduction of near surface transport and deposition to the Arctic due to anthropogenic emission reductions in Eurasia, and an increasing BC load mainly due to the emissions from East Asia, in agreement with observations and other modelling studies. On the other hand model simulations with constant anthropogenic emissions indicated how the effect of changing meteorology in the last decades may have also determined significant trends of BC transport to the Arctic, which can be as strong as the trends due to anthropogenic emission changes;

- The increasing trend of the anticyclonic circulation anomaly over the Arctic (negative phase of the NAO) determines a decrease of the pollution transport pathway from Eurasia to the Arctic, with a decrease in BC surface concentrations and deposition particularly in the Eastern Arctic. On the other hand, the NAO trend favours a stable vertical stratification which determines an increase of BC transport in the upper troposphere from East Asia and North America with increasing trend of total column BC concentrations over the entire Arctic Ocean;

- SB directly transport BC in the Arctic lower troposphere from central Europe. The increasing trend of the blocking frequency over Scandinavia favour the transport of air pollution directly from Europe to the Barents Sea with a significant increase of BC wet deposition over the entire Arctic Ocean. Also this pattern determines a decrease of pollution transport from East Eurasia to the Arctic and an overall decrease of BC

load over the entire Arctic upper troposphere, except over the Barents Sea where the surface concentration trends is strongly increasing;

- The ENSO pattern has a smaller and statistically less significant impact on the transport and deposition of BC to the Arctic;

- The combined impact of all three atmospheric patterns on BC wet deposition determines a significant increasing trend between 1980 and 2015 over almost the entire Arctic Ocean, the Barents Sea and Fram Strait, Greenland, Alaska and the Canadian Archipelago. A small significant decreasing trend is estimated the East Siberian and Laptev Seas. The BC load increases over the whole Arctic Ocean, with a significant trend only North of Greenland and the Barents Sea;

- The estimated interannual variability and trend of BC wet deposition over the Arctic Ocean is mainly driven by the SB pattern, with positive anomalies persisting for the last 10 years, 2005-2015. Smaller contributions are estimated for ENSO, only between 180°W-90°W, and NAO 90°W-0°. The interannual variability and trend of BC load over the Arctic is mainly driven by the NAO atmospheric patter, in particular north of the Barents Sea. In the other sectors of the Arctic, also SB contributes to the load total

variability.

- We have shown the robustness of a Bayesian approach to estimate the maximum likelihood distribution and trends of air pollutants associate to specific atmospheric patterns. The estimates obtained from different atmospheric reanalysis and global chemistry-climate model simulations are consistent. Problems may arise to resolve the total variability in presence of strong emission discontinuous changes. Although it

was possible to separate the effects of changing anthropogenic emissions from the meteorological variability using only global chemistry-climate simulations, by MLE further provided information on the feedback impacts of single atmospheric processes related to global warming and se ice retreat on pollution transport. By using outputs from existing coupled model simulations the method may be applied with other atmospheric processes related to the pollution transport and to other temporal intervals.

25 Our results show how sea ice retreat in winter and enhanced Arctic warming may indirectly and remotely impact the BC deposition on the sea ice itself. A negative feedback (decreasing BC deposition over the sea ice) is mainly over the area that in the recent years is characterized by the thin first-year sea ice, while the positive feedback (increasing sea ice deposition) is over the area with the thicker multiyear sea ice, which is becoming a smaller fraction of the total sea ice cover in last year's summers. During the winter polar night the deposited BC has no impact on the sea ice melting. When the sun appears in the

30 spring the short wave radiation starts to melt the fresh snow deposited on the sea ice. The BC impact on the albedo may be the most important at the end of the winter season, just before the snow starts to melt and surface becomes darker. Therefore, the BC deposition in winter may accelerate the initial melting of the snow and by an integrated effect it may result in the increased melting at the end of summer. The first-year sea ice may be completely melted every summer and the decrease of the BC deposition might not be the most important factor controlling its coverage in the late summer. On the other hand,

with the increased deposition of BC the multiyear sea ice may melt more and its thickness may become reduced with respect to the previous year. If this process happens consistently over several decades it might significantly contribute to reduction of the thickness of the multiyear sea ice. Our estimate of the temporal variability of the BC deposition over the multiyear sea ice indicates that the deposition in the winter due to the sea ice retreat feedback increased especially in the last ten years.

5 The increasing trend of the BC deposition emphasizes the importance of the reduction of BC anthropogenic emissions in the mid latitudes. In particular the SB pattern, which is closely related to the hemispheric warming, favours the transport to the Arctic Ocean of polluted air masses from the North Atlantic, which frequently originate from emissions in Europe and North America, and increased deposition on the multiyear sea ice. Policies that reduced anthropogenic emissions in the last decades, therefore, reduced the risk of a further acceleration of the melting of the multiyear sea ice. A strong shift of the 10 anthropogenic emissions from North America and Europe to East and South Asia also contributed to reduce the transport of BC to the Arctic from Eurasia, which represents the main transport pathway. We may have an indication of the impact of this geographical emissions shift by comparing the trends estimated using the FIX2000 and FIX1980 BC simulations (Figure S5). The BC deposition trend increased over the East Siberian and Laptev Sea considering the anthropogenic emissions of year 2000 compared to 1980, indicating that the contribution from the Asian emissions may play an important role in the 15 future. This increase is affecting deeper into the Arctic Ocean in particular in association with the NAO pattern. A similar impact of the increasing emissions in Asia was estimated for the BC burden, in particular associated to NAO and extending from Siberia, across the Arctic Ocean up to the Canadian Archipelago and Greenland.

In order to further understand the feedback between the global warming process and the trend of the BC deposition it will be necessary to extend the study to other seasons. In particular the major precipitation and wet deposition of BC happen in the 20 summer when also the reduction of the ice cover in the recent years is the largest. Furthermore, although the use of different estimates for atmospheric patterns and coupled atmosphere-chemistry relationships provides some information on their uncertainty, in the future the method will be applied with several coupled models to further assess the uncertainties. The same methodology may be also applied to estimate trends of BC transport to the Arctic associated to atmospheric circulation changes in the future, for example using the global climate simulations instead of atmospheric reanalysis.

25 **References**

Aoki, T., Aoki, T., Fukabori, M., Hachikubo, A., Tachibana, Y. and Nishio, F.: Effects of snow physical parameters on spectral albedo and bidirectional reflectance of snow surface, J. Geophys. Res., 105(D8), 10219, doi:10.1029/1999JD901122, 2000.

Auvray, M., Bey, I., Llull, E., Schultz, M. G. and Rast, S.: A model investigation of tropospheric ozone chemical tendencies 30 in long-range transported pollution plumes, J. Geophys. Res. Atmos., 112(5), 1–17, doi:10.1029/2006JD007137, 2007.

Barrie, L. A.: Arctic air pollution: An overview of current knowledge, Atmos. Environ., 20(4), 643–663, doi:http://dx.doi.org/10.1016/0004-6981(86)90180-0, 1986.

Byrd, R., Lu, P., Nocedal, J. and Zhu, C.: A Limited Memory Algorithm for Bound Constrained Optimization, SIAM J. Sci. Comput., 16(5), 1190–1208, doi:10.1137/0916069, 1995.

Cohen, J., Screen, J. a., Furtado, J. C., Barlow, M., Whittleston, D., Coumou, D., Francis, J., Dethloff, K., Entekhabi, D., Overland, J. and Jones, J.: Recent Arctic amplification and extreme mid-latitude weather, Nat. Geosci., 7(August), 627–637, doi:10.1038/ngeo2234, 2014.

Comiso, J. C.: Large decadal decline of the arctic multiyear ice cover, J. Clim., 25(4), 1176–1193, doi:10.1175/JCLI-D-11-00113.1, 2012.

Conway, H., Gades, A. and Raymond, C. F.: Albedo of dirty snow during conditions of melt did not persist for more than a few days . The migration of particles persisted for several weeks and , compared, , 32(6), 1713–1718, 1996.

Dee, D. P., Uppala, S. M., Simmons, A. J., Berrisford, P., Poli, P., Kobayashi, S., Andrae, U., Balmaseda, M. A., Balsamo, G., Bauer, P., Bechtold, P., Beljaars, A. C. M., van de Berg, L., Bidlot, J., Bormann, N., Delsol, C., Dragani, R., Fuentes, M., Geer, A. J., Haimberger, L., Healy, S. B., Hersbach, H., Holm, E. V., Isaksen, L., Kallberg, P., Kohler, M., Matricardi, M., Mcnally, A. P., Monge-Sanz, B. M., Morcrette, J. J., Park, B. K., Peubey, C., de Rosnay, P., Tavolato, C., Thepaut, J. N. and Vitart, F.: The ERA-Interim reanalysis: Configuration and performance of the data assimilation system, Q. J. R. Meteorol. Soc., 137(656), 553–597, doi:10.1002/qj.828, 2011.

Deser, C., Tomas, R. A. and Peng, S.: The transient atmospheric circulation response to North Atlantic SST and sea ice anomalies, J. Clim., 20(18), 4751–4767, doi:10.1175/JCLI4278.1, 2007.

Diehl, T., Heil, A., Chin, M., Pan, X., Streets, D., Schultz, M. and Kinne, S.: Anthropogenic, biomass burning, and volcanic emissions of black carbon, organic carbon, and SO2 from 1980 to 2010 for hindcast model experiments, Atmos. Chem. Phys. Discuss., 12, 24895–24954, doi:10.5194/acpd-12-24895-2012, 2012.

Dobricic, S., Vignati, E. and Russo, S.: Large scale atmospheric warming in winter and the Arctic sea ice retreat, J. Clim., 160215105924000, doi:10.1175/JCLI-D-15-0417.1, 2016.

Doscher, R., Vihma, T. and Maksimovich, E.: Recent advances in understanding the Arctic climate system state and change from a sea ice perspective: A review, Atmos. Chem. Phys., 14(24), 13571–13600, doi:10.5194/acp-14-13571-2014, 2014.

Endresen, Ø., Sørgard, E., Sundet, J., Dalsøren, S., Isaksen, I. and Berglen, T.: Emission from international sea transportation and environmental impact, J. Geophys. Res., 108(17), 14.1–14.22, doi:10.1029/2002JD002898, 2003.

Feldstein, S. B. and Lee, S.: Intraseasonal and interdecadal jet shifts in the Northern Hemisphere: The role of warm pool tropical convection and sea ice, J. Clim., 27(17), 6497–6518, doi:10.1175/JCLI-D-14-00057.1, 2014.

Flanner, M. G.: Arctic climate sensitivity to local black carbon, J. Geophys. Res. Atmos., 118(4), 1840–1851, doi:10.1002/jgrd.50176, 2013.

Flanner, M. G. and Zender, C. S.: Linking snowpack microphysics and albedo evolution, J. Geophys. Res. Atmos., 111(12), 1–12, doi:10.1029/2005JD006834, 2006.

Hadley, O. L. and Kirchstetter, T. W.: Black-carbon reduction of snow albedo, Nat. Clim. Chang., 2(6), 437–440, doi:10.1038/nclimate1433, 2012.

Hannachi, A., Unkel, S., Trendafilov, N. T. and Jolliffe, I. T.: Independent component analysis of climate data: A new look at EOF rotation, J. Clim., 22(11), 2797–2812, doi:10.1175/2008JCLI2571.1, 2009.

Hirdman, D., Burkhart, J. F., Sodemann, H., Eckhardt, S., Jefferson, A., Quinn, P. K., Sharma, S., Ström, J. and Stohl, A.: Long-term trends of black carbon and sulphate aerosol in the Arctic: Changes in atmospheric transport and source region emissions, Atmos. Chem. Phys., 10(19), 9351–9368, doi:10.5194/acp-10-9351-2010, 2010.

Hyvärinen, A. and Oja, E.: Independent component analysis: Algorithms and applications, Neural Networks, 13(4-5), 411–430, doi:10.1016/S0893-6080(00)00026-5, 2000.

Kalnay, E., Kanamitsu, M., Kistler, R., Collins, W., Deaven, D., Gandin, L., Iredell, M., Saha, S., White, G., Woollen, J., Zhu, Y., Chelliah, M., Ebisuzaki, W., Higgins, W., Janowiak, J., Mo, K. C., Ropelewski, C., Wang, J., Leetmaa, A., Reynolds, R., Jenne, R. and Joseph, D.: The NCEP/NCAR 40-year reanalysis project, Bull. Am. Meteorol. Soc., 77(3), 437–471, doi:10.1175/1520-0477(1996)077<0437:TNYRP>2.0.CO;2, 1996.

Kim, D., Chin, M., Yu, H., Diehl, T., Tan, Q., Kahn, R. A., Tsigaridis, K., Bauer, S. E., Takemura, T., Pozzoli, L., Bellouin, N., Schulz, M., Peyridieu, S., Chédin, A. and Koffi, B.: Sources, sinks, and transatlantic transport of North African dust aerosol: A multimodel analysis and comparison with remote sensing data, J. Geophys. Res. Atmos., 119(10), 6259–6277, doi:10.1002/2013JD021099, 2014.

Klonecki, A.: Seasonal changes in the transport of pollutants into the Arctic troposphere-model study, J. Geophys. Res., 108(D4), 8367, doi:10.1029/2002JD002199, 2003.

Kwok, R.: Outflow of Arctic Ocean Sea Ice into the Greenland and Barents Seas: 1979–2007, J. Clim., 22(9), 2438–2457, doi:10.1175/2008JCLI2819.1, 2009.

Kwok, R. and Rothrock, D. A.: Decline in Arctic sea ice thickness from submarine and ICESat records: 1958-2008, Geophys. Res. Lett., 36(15), 1–5, doi:10.1029/2009GL039035, 2009.

Mann, H. B.: Nonparametric Tests Against Trend, Econometrica, 13(3), 245–259, doi:10.2307/1907187, 1945.

Maslanik, J., Stroeve, J., Fowler, C. and Emery, W.: Distribution and trends in Arctic sea ice age through spring 2011, Geophys. Res. Lett., 38(13), 2–7, doi:10.1029/2011GL047735, 2011.

Mori, M., Watanabe, M., Shiogama, H., Inoue, J. and Kimoto, M.: Robust Arctic sea-ice influence on the frequent Eurasian cold winters in past decades, Nat. Geosci., 7(October 2014), 869–874, doi:10.1038/ngeo2277, 2014.

Overland, J. E. and Wang, M.: Large-scale atmospheric circulation changes are associated with the recent loss of Arctic sea ice, Tellus, Ser. A Dyn. Meteorol. Oceanogr., 62(1), 1–9, doi:10.1111/j.1600-0870.2009.00421.x, 2010.

Pan, X., Chin, M., Gautam, R., Bian, H., Kim, D., Colarco, P. R., Diehl, T. L., Takemura, T., Pozzoli, L., Tsigaridis, K., Bauer, S. and Bellouin, N.: A multi-model evaluation of aerosols over South Asia: Common problems and possible causes, Atmos. Chem. Phys., 15(10), 5903–5928, doi:10.5194/acp-15-5903-2015, 2015.

Pausata, F. S. R., Pozzoli, L., Vignati, E. and Dentener, F. J.: North Atlantic Oscillation and tropospheric ozone variability in Europe: Model analysis and measurements intercomparison, Atmos. Chem. Phys., 12(14), 6357–6376, doi:10.5194/acp-12-6357-2012, 2012.

Pausata, F. S. R., Pozzoli, L., Dingenen, R. Van, Vignati, E., Cavalli, F. and Dentener, F. J.: Impacts of changes in North Atlantic atmospheric circulation on particulate matter and human health in Europe, Geophys. Res. Lett., 40(15), 4074–4080, 2013.

Petoukhov, V. and Semenov, V. A.: A link between reduced Barents-Kara sea ice and cold winter extremes over northern continents, J. Geophys. Res. Atmos., 115(21), 1–11, doi:10.1029/2009JD013568, 2010.

Pozzoli, L., Bey, I., Rast, S., Schultz, M. G., Stier, P. and Feichter, J.: Trace gas and aerosol interactions in the fully coupled model of aerosol-chemistry-climate ECHAM5-HAMMOZ: 1. Model description and insights from the spring 2001 TRACE-P experiment, J. Geophys. Res. Atmos., 113(7), doi:10.1029/2007JD009007, 2008a.

Pozzoli, L., Bey, I., Rast, S., Schultz, M. G., Stier, P. and Feichter, J.: Trace gas and aerosol interactions in the fully coupled model of aerosol-chemistry-climate ECHAM5-HAMMOZ: 2. Impact of heterogeneous chemistry on the global aerosol distributions, J. Geophys. Res. Atmos., 113(7), 1–15, doi:10.1029/2007JD009008, 2008b.

Pozzoli, L., Janssens-Maenhout, G., Diehl, T., Bey, I., Schultz, M. G., Feichter, J., Vignati, E. and Dentener, F.: Re-analysis of tropospheric sulfate aerosol and ozone for the period 1980-2005 using the aerosol-chemistry-climate model ECHAM5-HAMMOZ, Atmos. Chem. Phys., 11(18), 9563–9594, 2011.

Rothrock, D. A., Percival, D. B. and Wensnahan, M.: The decline in arctic sea-ice thickness: Separating the spatial, annual, and interannual variability in a quarter century of submarine data, J. Geophys. Res. Ocean., 113(5), 1–9, doi:10.1029/2007JC004252, 2008.

Sand, M., Berntsen, T. K., Seland, Ø. and Kristjánsson, J. E.: Arctic surface temperature change to emissions of black carbon within Arctic or midlatitudes, J. Geophys. Res. Atmos., 118(14), 7788–7798, doi:10.1002/jgrd.50613, 2013a.

Sand, M., Berntsen, T. K., Kay, J. E., Lamarque, J. F., Seland and Kirkeväg, A.: The arctic response to remote and local forcing of black carbon, Atmos. Chem. Phys., 13(1), 211–224, doi:10.5194/acp-13-211-2013, 2013b.

Sand, M., Berntsen, T. K., von Salzen, K., Flanner, M. G., Langner, J. and Victor, D. G.: Response of Arctic temperature to changes in emissions of short-lived climate forcers, Nat. Clim. Chang., 6(November), 1–5, doi:10.1038/nclimate2880, 2015.

Sato, K., Inoue, J. and Watanabe, M.: Influence of the Gulf Stream on the Barents Sea ice retreat and Eurasian coldness during early winter, , 9(8), doi:10.1088/1748-9326/9/8/084009, 2014.

Schultz, M. G., Heil, A., Hoelzemann, J. J., Spessa, A., Thonicke, K., Goldammer, J. G., Held, A. C., Pereira, J. M. C. and van Het Bolscher, M.: Global wildland fire emissions from 1960 to 2000, Global Biogeochem. Cycles, 22(2), 1–17, doi:10.1029/2007GB003031, 2008.

Screen, J. A., Simmonds, I., Deser, C. and Tomas, R.: The atmospheric response to three decades of observed arctic sea ice loss, J. Clim., 26(4), 1230–1248, doi:10.1175/JCLI-D-12-00063.1, 2013.

Semenov, V. A. and Latif, M.: Nonlinear winter atmospheric circulation response to Arctic sea ice concentration anomalies for different periods during 1966–2012, Environ. Res. Lett., 10(5), 054020, doi:10.1088/1748-9326/10/5/054020, 2015.

Sen, P. K.: Estimates of the Regression Coefficient Based on Kendall's Tau, J. Am. Stat. Assoc., 63(324), 1379–1389, doi:10.2307/2285891, 1968.

Serreze, M. C. and Barry, R. G.: Processes and impacts of Arctic amplification: A research synthesis, Glob. Planet. Change, 77(1-2), 85–96, doi:10.1016/j.gloplacha.2011.03.004, 2011.

Sharma, S., Ishizawa, M., Chan, D., Lavoué, D., Andrews, E., Eleftheriadis, K. and Maksyutov, S.: 16-year simulation of Arctic black carbon : Transport , source contribution , and sensitivity analysis on deposition, , 118, 943–964, doi:10.1029/2012JD017774, 2013.

Shaw, G. E. and Stamnes, K.: ARCTIC HAZE: PERTURBATION OF THE POLAR RADIATION BUDGET*, Ann. N. Y. Acad. Sci., 338(1), 533–539, doi:10.1111/j.1749-6632.1980.tb17145.x, 1980.

Shindell, D. and Faluvegi, G.: Climate response to regional radiative forcing during the twentieth century, Nat. Geosci, 2(4), 294–300 [online] Available from: http://dx.doi.org/10.1038/ngeo473, 2009.

Shindell, D., Kuylenstierna, J. C. I., Vignati, E., van Dingenen, R., Amann, M., Klimont, Z., Anenberg, S. C., Muller, N., Janssens-Maenhout, G., Raes, F., Schwartz, J., Faluvegi, G., Pozzoli, L., Kupiainen, K., Hoglund-Isaksson, L., Emberson, L., Streets, D., Ramanathan, V., Hicks, K., Oanh, N. T. K., Milly, G., Williams, M., Demkine, V. and Fowler, D.: Simultaneously Mitigating Near-Term Climate Change and Improving Human Health and Food Security, Science (80-.)., 335(6065), 183–189, doi:10.1126/science.1210026, 2012.

Stier, P., Feichter, J., Kinne, S., Kloster, S., Vignati, E., Wilson, J., Ganzeveld, L., Tegen, I., Werner, M., Balkanski, Y., Schulz, M. and Boucher, O.: The aerosol-climate model ECHAM5-HAM, Atmos. Chem. Phys. Discuss., 4(5), 5551–5623, doi:10.5194/acpd-4-5551-2004, 2005.

Stohl, A.: Characteristics of atmospheric transport into the Arctic troposphere, J. Geophys. Res. Atmos., 111(11), 1–17, doi:10.1029/2005JD006888, 2006.

Tsigaridis, K., Daskalakis, N., Kanakidou, M., Adams, P. J., Artaxo, P., Bahadur, R., Balkanski, Y., Bauer, S. E., Bellouin, N., Benedetti, A., Bergman, T., Berntsen, T. K., Beukes, J. P., Bian, H., Carslaw, K. S., Chin, M., Curci, G., Diehl, T., Easter, R. C., Ghan, S. J., Gong, S. L., Hodzic, A., Hoyle, C. R., Iversen, T., Jathar, S., Jimenez, J. L., Kaiser, J. W., Kirkeväg, A., Koch, D., Kokkola, H., H Lee, Y., Lin, G., Liu, X., Luo, G., Ma, X., Mann, G. W., Mihalopoulos, N., Morcrette, J. J., Müller, J. F., Myhre, G., Myriokefalitakis, S., Ng, N. L., O'donnell, D., Penner, J. E., Pozzoli, L., Pringle, K. J., Russell, L. M., Schulz, M., Sciare, J., Seland, Shindell, D. T., Sillman, S., Skeie, R. B., Spracklen, D., Stavrakou, T., Steenrod, S. D., Takemura, T., Tiitta, P., Tilmes, S., Tost, H., Van Noije, T., Van Zyl, P. G., Von Salzen, K., Yu, F., Wang, Z., Wang, Z., Zaveri, R. A., Zhang, H., Zhang, K., Zhang, Q. and Zhang, X.: The AeroCom evaluation and intercomparison of organic aerosol in global models, Atmos. Chem. Phys., 14(19), 10845–10895, doi:10.5194/acp-14-10845-2014, 2014.

Uppala, S. M., KÅllberg, P. W., Simmons, A. J., Andrae, U., Bechtold, V. D. C., Fiorino, M., Gibson, J. K., Haseler, J., Hernandez, A., Kelly, G. A., Li, X., Onogi, K., Saarinen, S., Sokka, N., Allan, R. P., Andersson, E., Arpe, K., Balmaseda, M. A., Beljaars, A. C. M., Berg, L. Van De, Bidlot, J., Bormann, N., Caires, S., Chevallier, F., Dethof, A., Dragosavac, M., Fisher, M., Fuentes, M., Hagemann, S., Hólm, E., Hoskins, B. J., Isaksen, L., Janssen, P. A. E. M., Jenne, R., Mcnally, A. P., Mahfouf, J.-F., Morcrette, J.-J., Rayner, N. A., Saunders, R. W., Simon, P., Sterl, A., Trenberth, K. E., Untch, A., Vasiljevic, D., Viterbo, P. and Woollen, J.: The ERA-40 re-analysis, Q. J. R. Meteorol. Soc., 131(612), 2961–3012,

doi:10.1256/qj.04.176, 2005.

Yasunari, T. J., Koster, R. D., Lau, K. M., Aoki, T., Sud, Y. C., Yamazaki, T., Motoyoshi, H. and Kodama, Y.: Influence of dust and black carbon on the snow albedo in the NASA Goddard Earth Observing System version 5 land surface model, J. Geophys. Res. Atmos., 116(2), 1–15, doi:10.1029/2010JD014861, 2011.

Table 1: Combination of atmospheric reanalysis, global chemistry-climate model simulations and time periods used to generate MLE of BC deposition and load.

Estimate name	Atmospheric reanalysis	BC simulation	Period
NCEP-2000-A	NCEP	FIX2000	1980-2005
ERA-2000-A	ERA-Interim	FIX2000	1980-2005
NCEP-1980-A	NCEP	FIX1980	1980-2005
ERA-1980-A	ERA-Interim	FIX1980	1980-2005
NCEP-REF-B	NCEP	REF	1993-2005
ERA-REF-B	ERA-Interim	REF	1993-2005
NCEP-2000-B	NCEP	FIX2000	1993-2005
ERA-2000-B	ERA-Interim	FIX2000	1993-2005

a) Wet Dep. [kg/year] REF
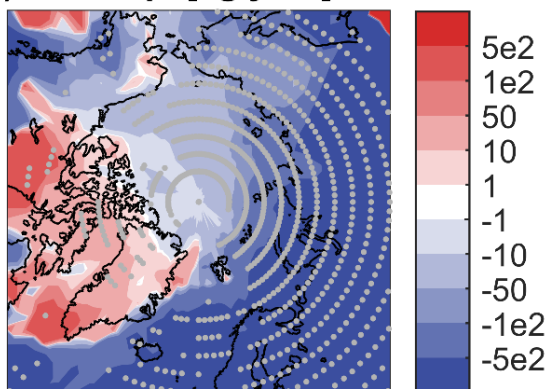
b) Dry Dep. [10^{-3} kg/year] REF
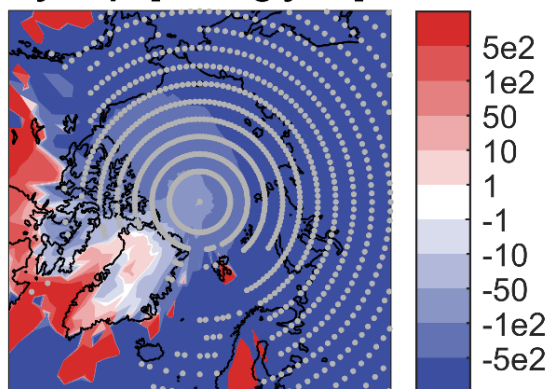
c) Srf.Conc. [10^{-3} ng/kg/year] REF
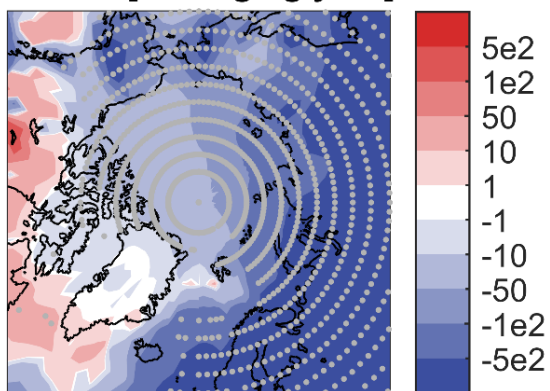
d) Load [10^{-2} kg/year] REF
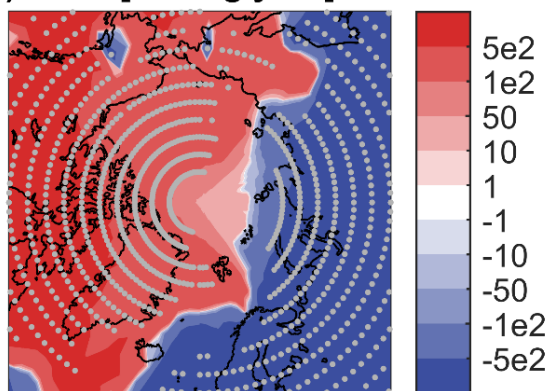
Figure 1 Winter (DJF) trends of BC wet deposition (a), dry deposition (b), surface concentration (d), and total load (d) for the ECHAM5-HAMMOZ REF simulation. Grey dots represent the grid points with trend significant at 5% level.

a) Wet Dep. [kg/year] FIX2000
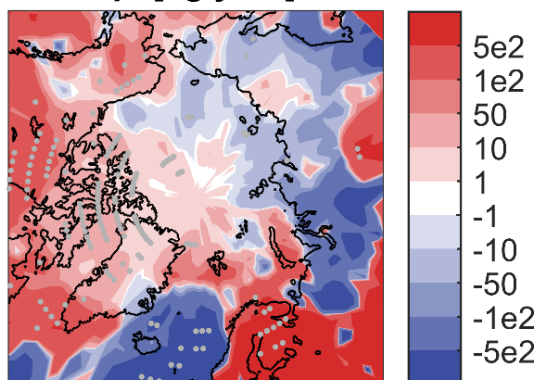
b) Dry Dep. [10^{-3} kg/year] FIX2000
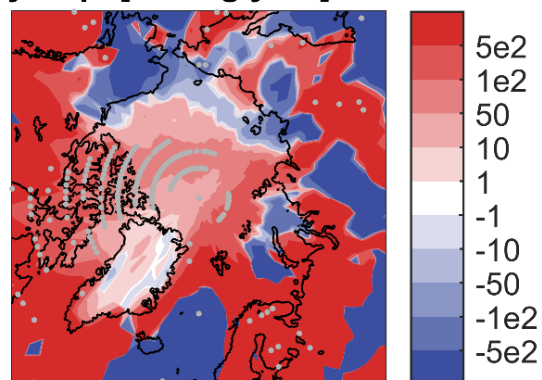
c) Srf.Conc. [10^{-3} ng/kg/year] FIX2000
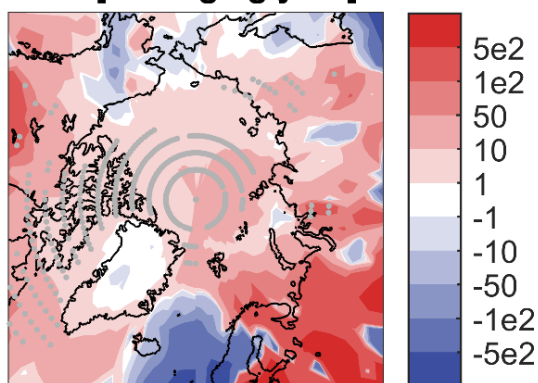
d) Load [10^{-2} kg/year] FIX2000
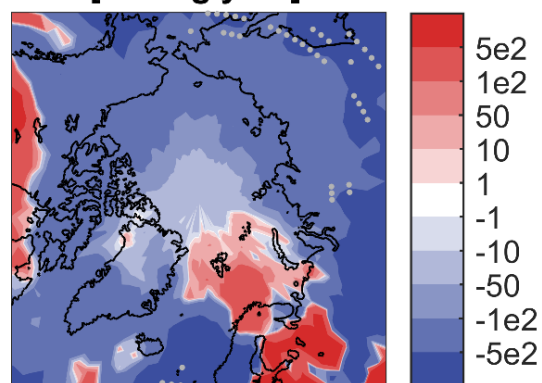
Figure 2 Winter (DJF) trends of BC wet deposition (a), dry deposition (b), surface concentration (d), and total load (d) for the ECHAM5-HAMMOZ FIX2000 simulation. Grey dots represent the grid points with trend significant at 5% level.
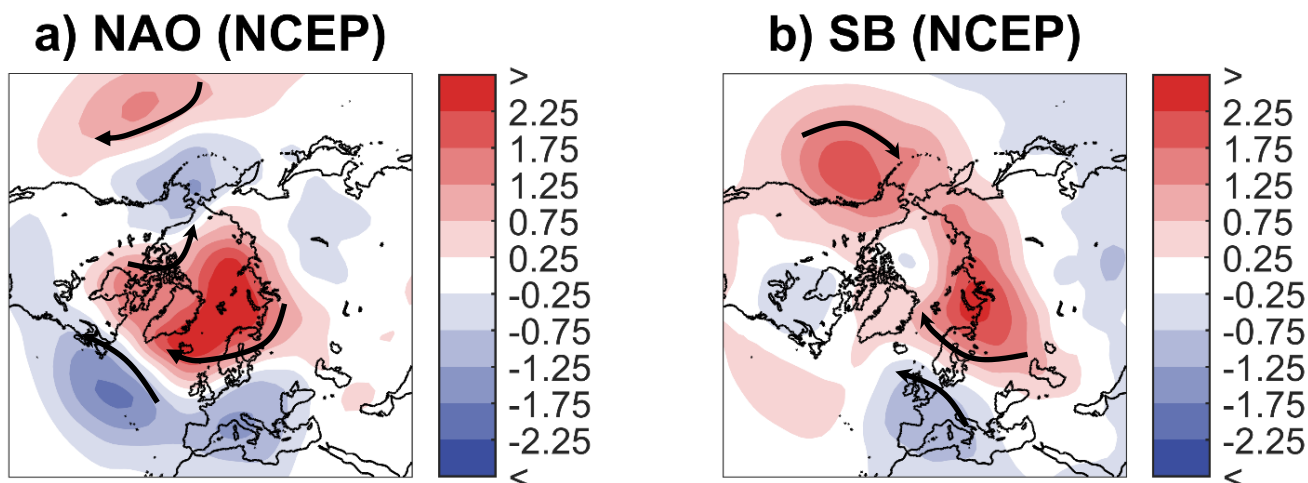
Figure 3 Trends associated to a) North Atlantic Oscillation (NAO) and b) Scandinavian Blocking (SB) patterns of geopotential height at 850mb isobaric surface positioned about 1500m above the sea level from 1980-2015 (10^{-2} m year^{-1}). The arrows indicate the air circulation tendencies and transport of pollutants.
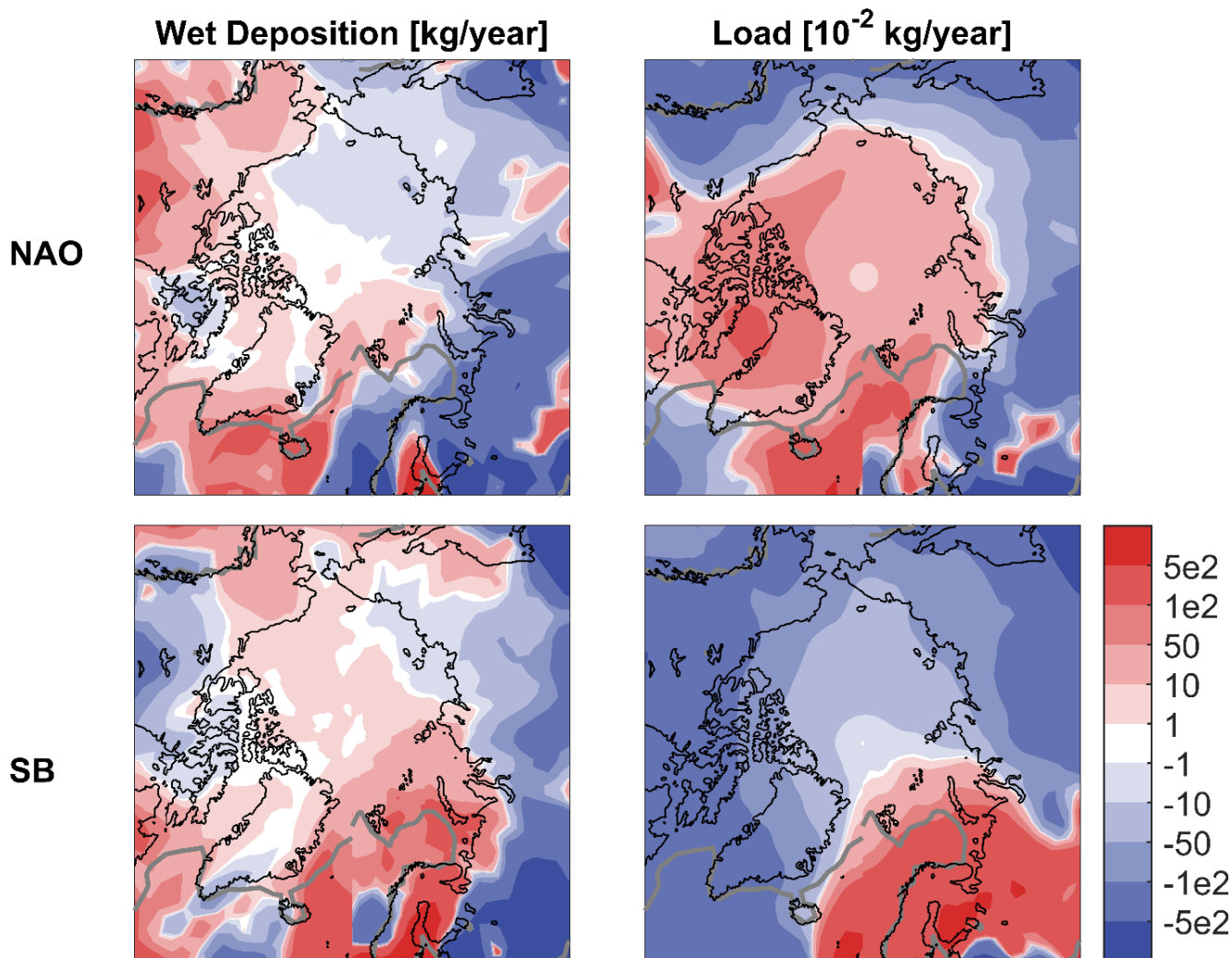
Figure 4 Trends of maximum likelihood estimates (MLE) of BC wet deposition (kg/year) and load (kg x 10^{-2}/year) associated to NAO and SB. The grey line represents the mean winter sea ice and snow cover larger than 50% since 1980 to now. NAO and SB trends are both significant at 5% level.

Trends of BC concentrations due to NAO
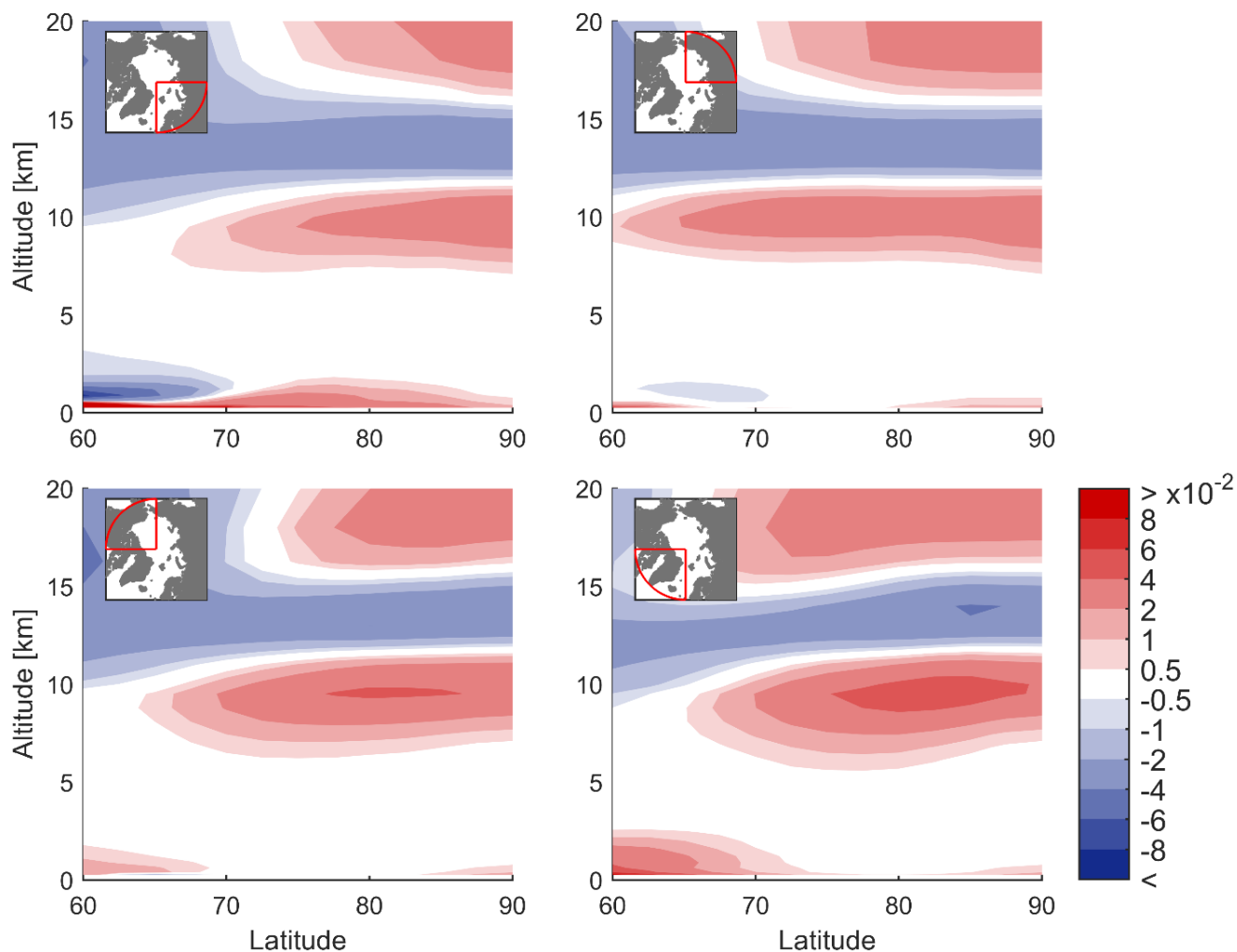
Figure 5 Trends of maximum likelihood estimates of BC concentrations (ng/kg/year) associated to NAO circulation pattern. BC concentrations at each model vertical level and latitudes above 60°N are averaged over 90° longitudes segments of the Arctic, indicated in the map on the left upper corner of each plot.

Trends of BC concentrations due to SB
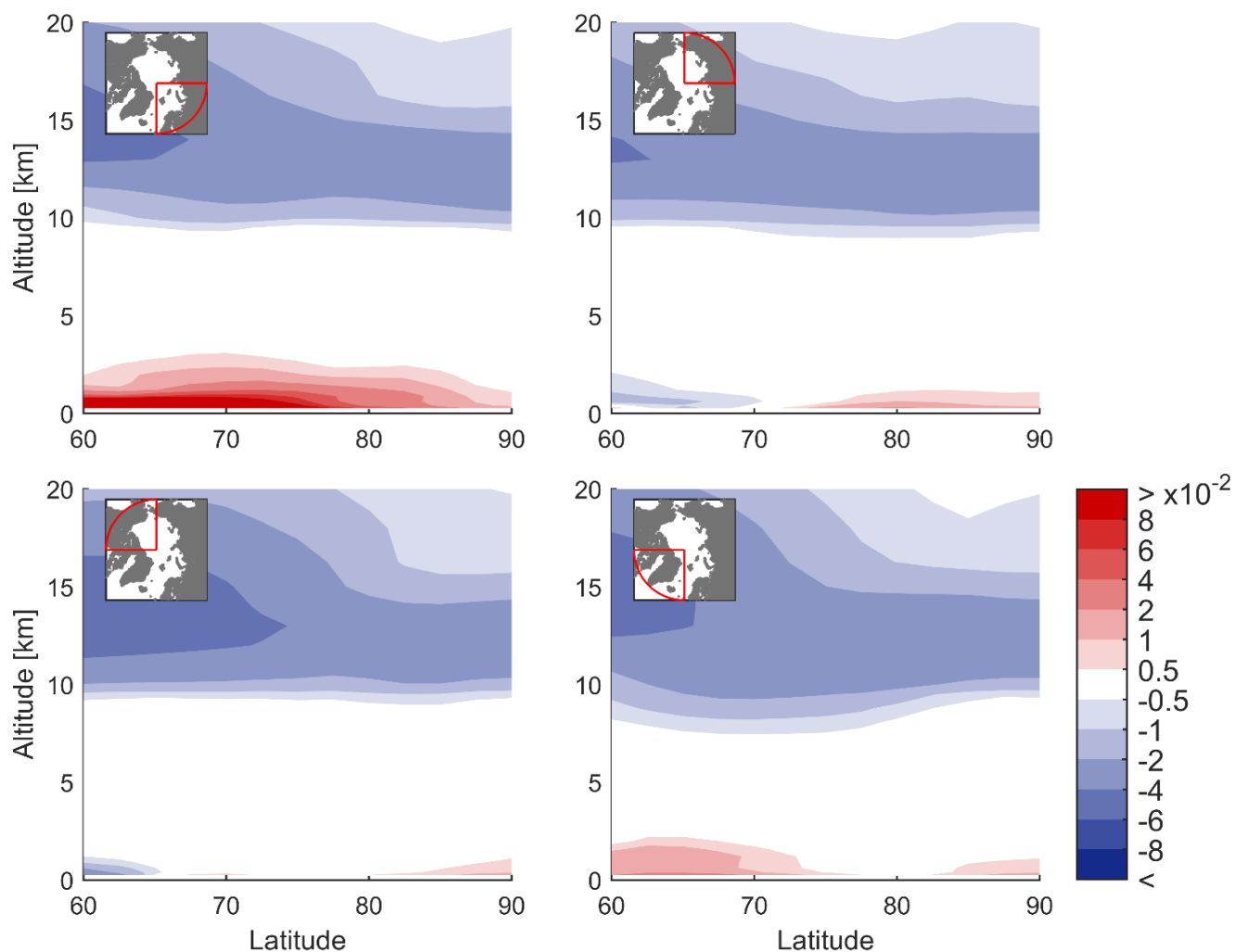
Figure 6 Trends of maximum likelihood estimates of BC concentrations (ng/kg/year) associated to SB circulation pattern. BC concentrations at each model vertical level and latitudes above 60°N are averaged over 90° longitudes segments of the Arctic, indicated in the map on the left upper corner of each plot.
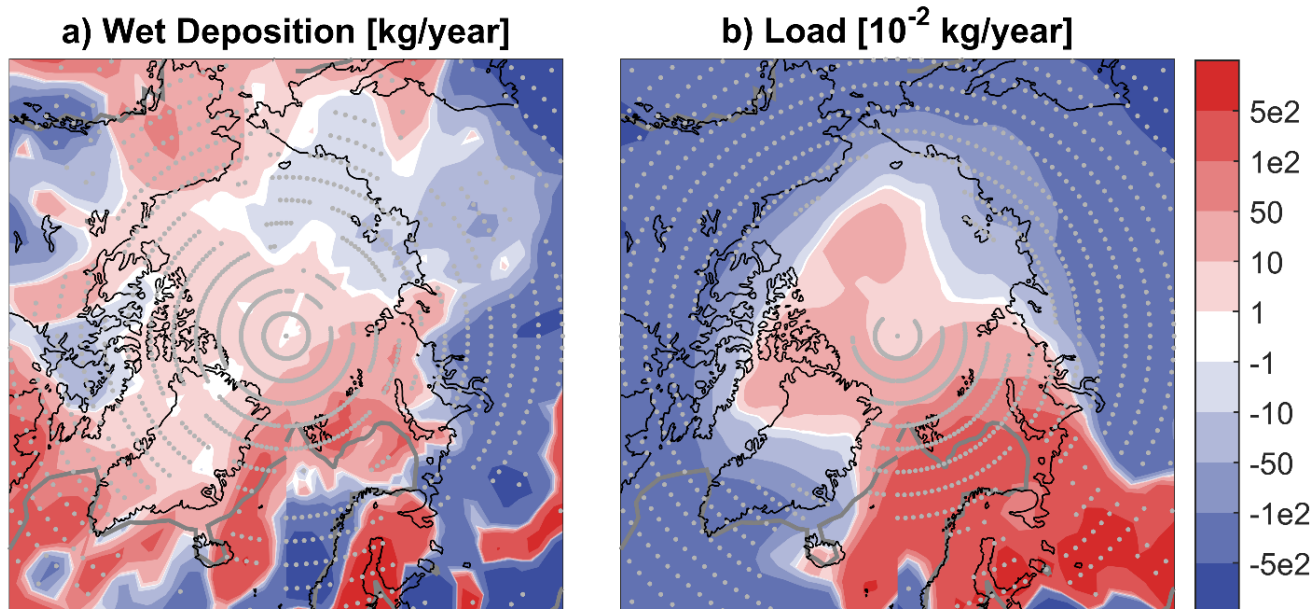
Figure 7 Total trends of maximum likelihood estimates (MLE) of BC wet deposition (kg/year) and load (kg x 10⁻²/year) associated to three atmospheric circulation patterns (Total=NAO+SB+ENSO). The grey line represents the mean winter sea ice and snow cover larger than 50% since 1980 to now. Grey dots represent the grid points with trend significant at 5% level.
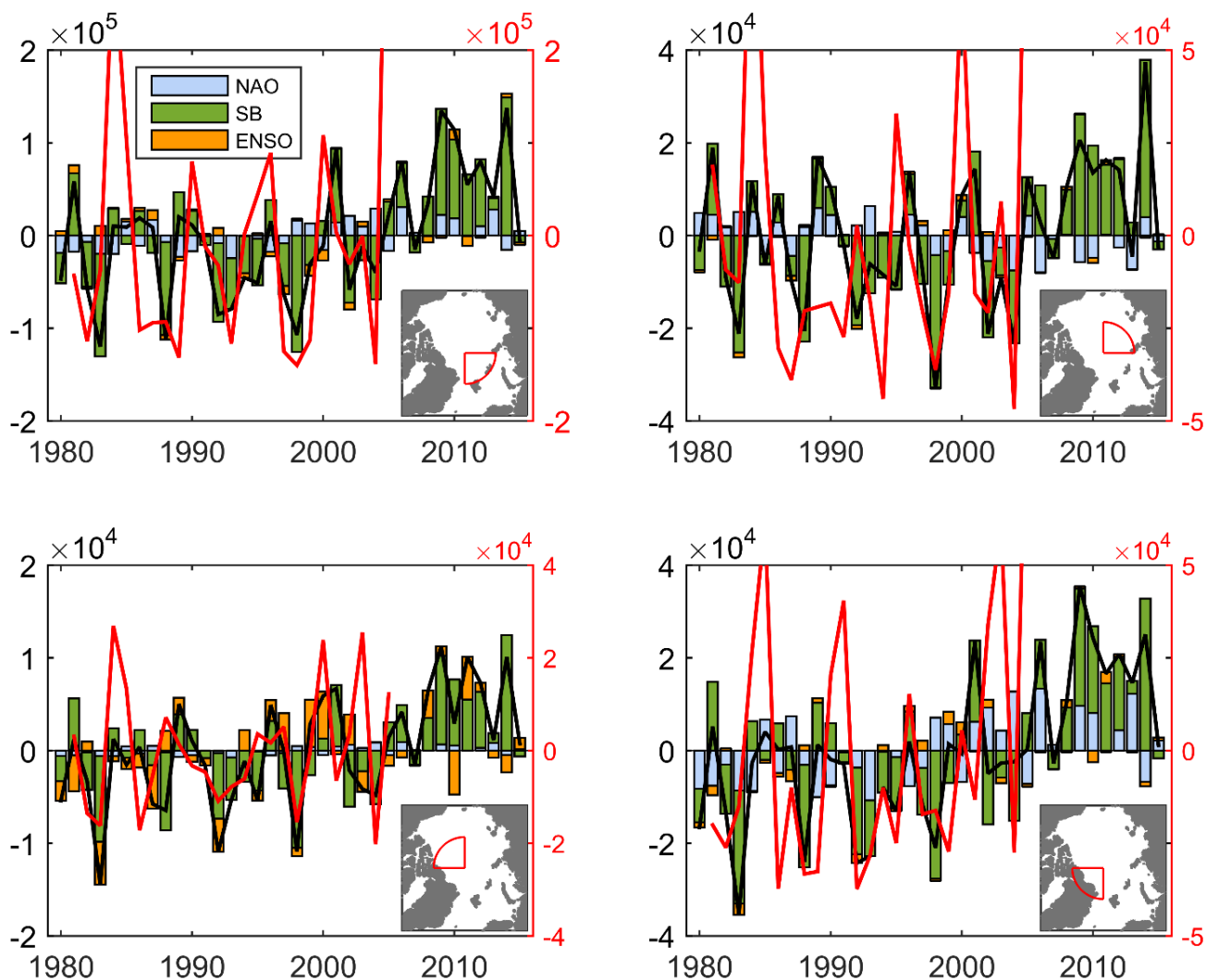
Figure 8 Temporal variability of total BC wet deposition anomaly over 90° longitude segments of the Arctic and between 80°N-90°N (kg/year) related to the circulation patterns NAO, SB and ENSO. The black line is the sum of the three components, the red line (right y-axis) is the total BC wet deposition anomaly from the FIX2000 simulation.
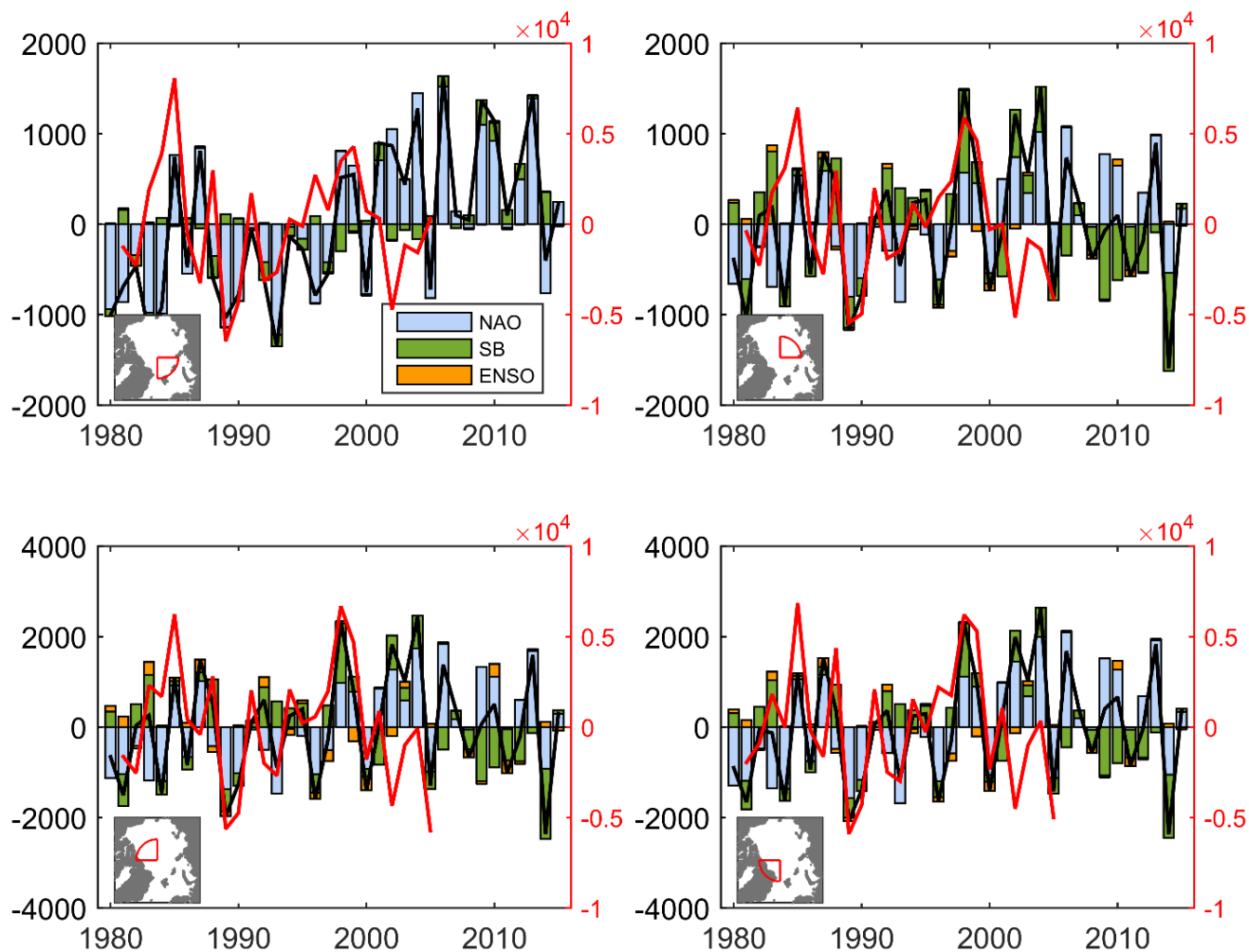
Figure 9 Temporal variability of total BC load anomaly over 90° longitude segments of the Arctic and between 80°N-90°N (kg/year) related to the circulation patterns NAO, SB and ENSO. The black line is the sum of the three components, the red line (right y-axis) is the total BC load anomaly from the FIX2000 simulation.

BC Wet Deposition [kg/year]
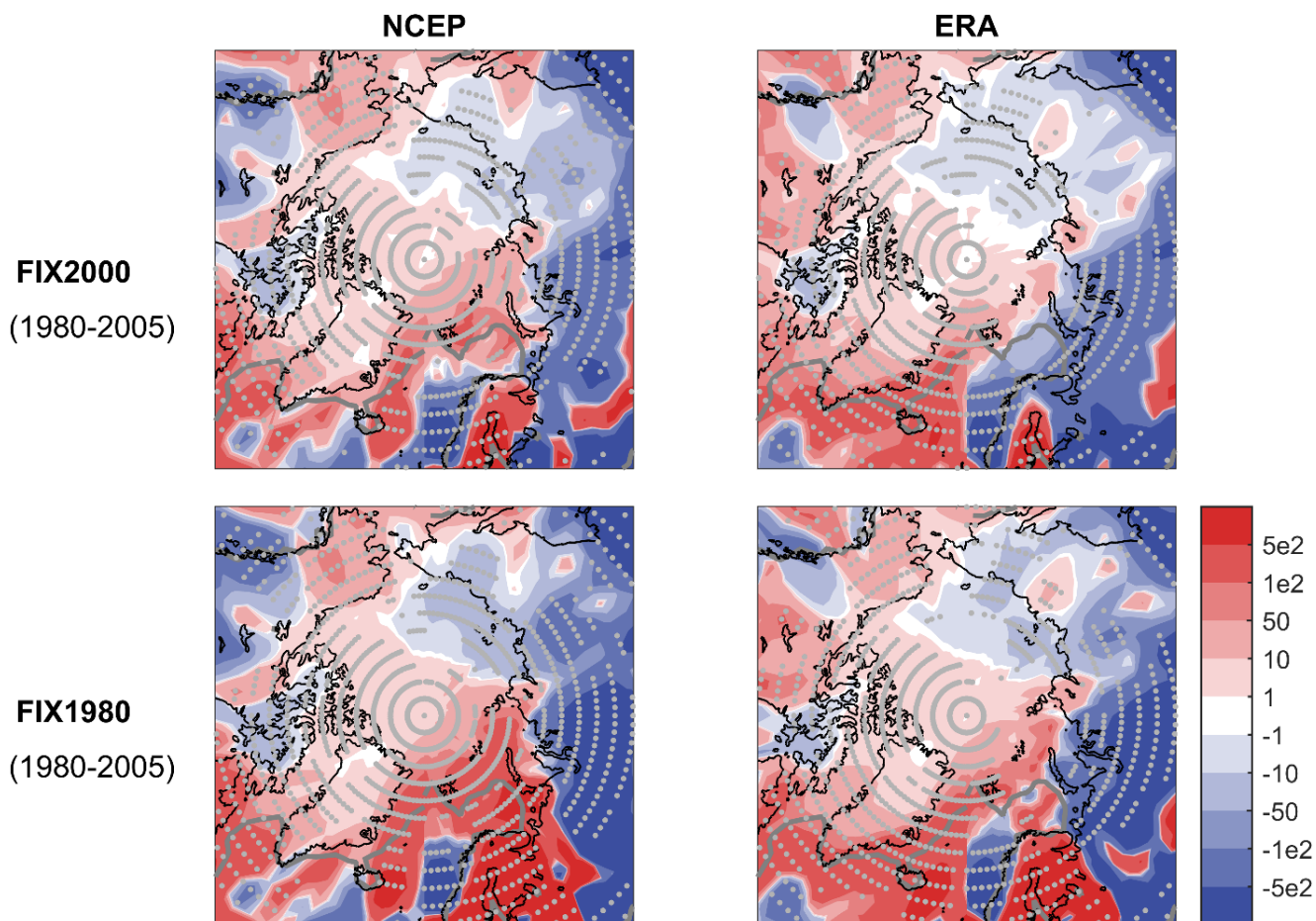
Figure 10 Four different estimates (see also Table 1) of total trends of maximum likelihood BC wet deposition (kg/year) associated to three atmospheric circulation patterns (Total=NAO+SB+ENSO). The grey line represents the mean winter sea ice and snow cover larger than 50% since 1980 to now. Grey dots represent the grid points with trend significant at 5% level.
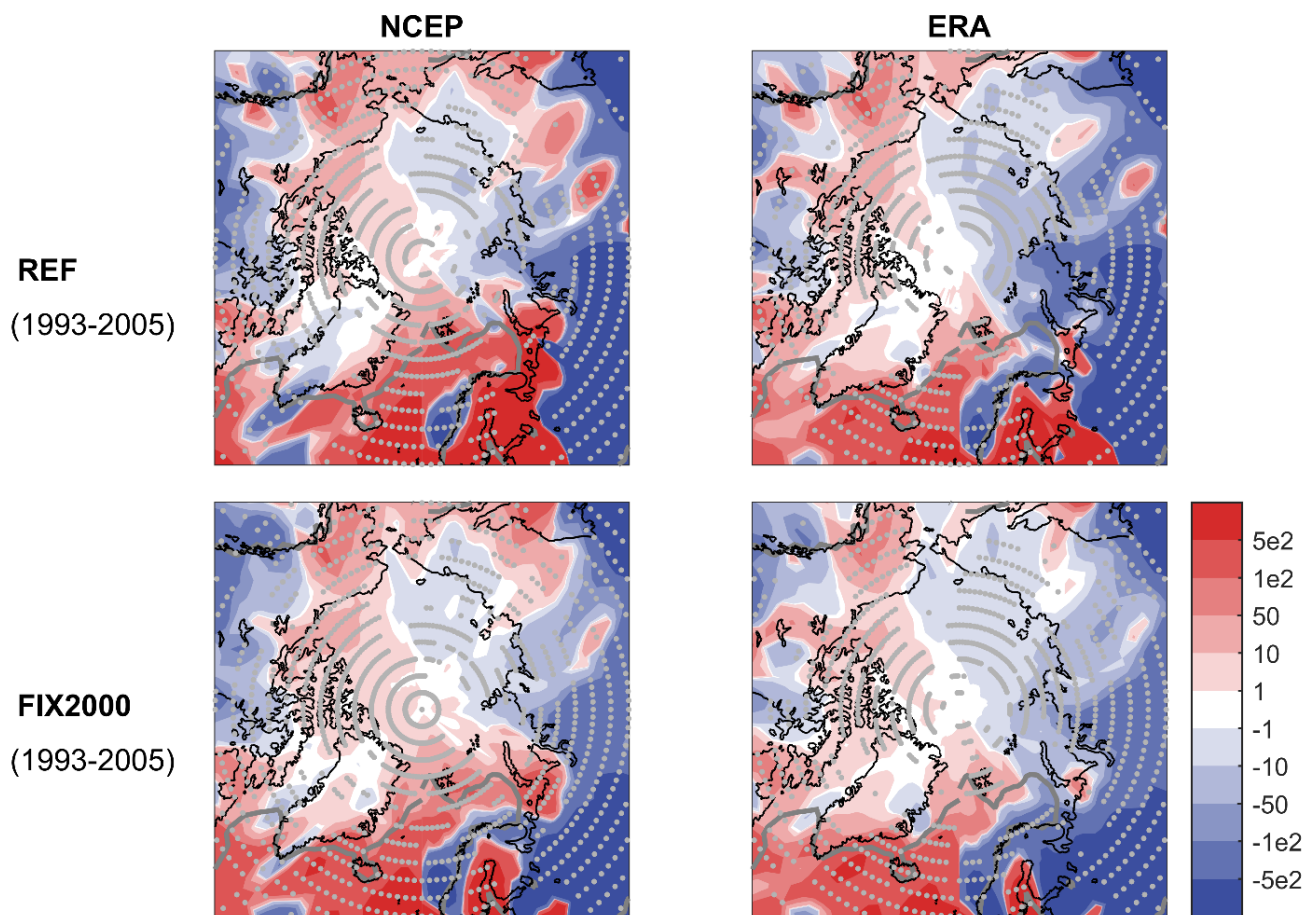
Figure 11 Four different estimates (see also Table 1) of total trends of maximum likelihood BC wet deposition (kg/year) associated to three atmospheric circulation patterns (Total=NAO+SB+ENSO). The grey line represents the mean winter sea ice and snow cover larger than 50% since 1980 to now. Grey dots represent the grid points with trend significant at 5% level.